Landslides triggered by the December 24, 2019 Mesetas (Meta, Colombia) Earthquake

Helbert García Delgado [a, *]; Jorge Chaparro [a, **]; Carlos Gamboa [a, ***]; Gloria Ruiz [a, ****]

[a] *Grupo de Evaluación de Amenaza por Movimientos en Masa, Servicio Geológico Colombiano, Bogotá - Colombia*

**hsgarcia@sgc.gov.co; helbertgarciad@gmail.com; **jchaparro@sgc.gov.co; ***cgamboa@sgc.gov.co; ****gruiz@sgc.gov.co*

Abstract

Among the environmental effects produced after earthquakes, landslides are one of the most significant geohazards to civil infrastructure or even to human life. Hence, the detailed understanding of contributing factors and the size-frequency distribution of earthquake-triggered landslides (EQTLs) is critical for future hazard analysis and risk mitigation efforts.

The Colombian Andes is one of the most actively seismogenic regions in South America, with records of recent destructive earthquakes such as the Popayán (Mw = 5.6; March 31, 1983), the Páez (Mw = 6.8; June 6, 1994) or the Armenia (Mw = 6.1; January 25, 1999) earthquakes. To date, a comprehensive EQTL inventory and even more analysis of both topographic and seismic parameters are still needed. This paper deals with an EQTL inventory from the Colombian Andes related to the Mesetas Earthquake (Mw = 6.0). According to the Red Sismológica Nacional de Colombia (RSNC) of the Dirección de Geoamenazas of the Servicio Geológico Colombiano (SGC), the Mesetas Earthquake struck the eastern foothills of the Eastern Cordillera of Colombia on December 24, 2019 (19:03:52 UTC) at a depth of about 13±2.9 km. For the Mesetas Earthquake, this contribution documents 838 EQTLs after performing a remote sensing analysis on both pre- and post-earthquake medium to high-resolution satellite imagery accompanied by fieldwork. Based on this inventory, the size-frequency distribution, the total affected area, and the relationship between landslides with both terrain (elevation, slope, relief, aspect, curvature, and the topographic position index) and seismic parameters (distance to the epicenter and distance to seismogenic fault) are discussed.

Based on the results, structure, and lithology, along with the steepest topography, are considered as the main factors contributing to the occurrence of EQTLs in the study area. Accordingly, peaks in landslide concentration and the mean landslide orientation were controlled by the shear zone bounded by the Guapecito Fault, a subsidiary branch of the Algeciras Fault, the structure responsible for the Mesetas Earthquake. It is inferred thus that tectonic weakening on the parental material, probably related to the seismic shaking of past earthquakes, is the main factor controlling the occurrence of EQTLs.

1 INTRODUCTION

In mountainous landscapes, landslides are one of the most significant natural hazards to human settlements. Indeed, more than 55,000 people died in the period spanning from 2004 to 2016 in non-seismic landslides (Froude and Petley, 2018). In the case of earthquake-triggered landslides (EQTLs), this phenomenon can be more dangerous to human life than ground shaking itself (Bird and Bommer, 2004; Budimir et al., 2014) accounting for almost 70% of non-shaking deaths (Marano et al., 2010). For instance, the Páez Earthquake on June 6, 1994 (Mw = 6.8), triggered more than 3,000 landslides (INGEOMINAS, 1996) that, in turn, feed a destructive debris flow that killed more than 1,100 people in southwest Colombia (Forero-Dueñas, 1996).

Given the importance of EQTLs on society, several authors have explored the relationship between EQTL and their conditioning factors, as well as their association with seismic parameters (Rodríguez et al. 1999). Among the seismic parameters, those related to the distance to the epicenter, distance to fault rupture, and co-seismic slip have been the most widely used to understand landslide distribution better (e.g., Keefer, 2000; Gorum et al., 2011).

Even though the Colombian Andes is one of the most actively seismogenic regions in South America, with records of destructive earthquakes such as the 1983 Popayán, the 1994 Páez, or the 1999 Armenia earthquakes, to date a comprehensive analysis of EQTL with both topographic and seismic parameters is still needed. This paper deals with an EQTL inventory from the Colombian Andes related to the Mesetas Earthquake (Mw = 6.0). According to Mayorga et al. (2020), the earthquake struck the eastern foothills of the Eastern Cordillera of Colombia (Figure 1) on December 24, 2019 (19:03:52 UTC) at a depth of about 13±2.9 km. Following the main event, an aftershock of Mw = 5.8 struck 16 minutes later (Mayorga et al., 2020).

For the Mesetas event, this contribution documents more than 800 EQTL after performing a remote sensing analysis on both pre- and post-earthquake medium to high-resolution satellite imagery accompanied by fieldwork. Based on this inventory, the size-frequency distribution, the total affected area, and the relationship between landslides with both seismic and terrain variables are discussed. Hence, this paper affords valuable information to future seismic hazard assessment projects in the mountainous regions of Colombia, where similar earthquakes are forecasted.

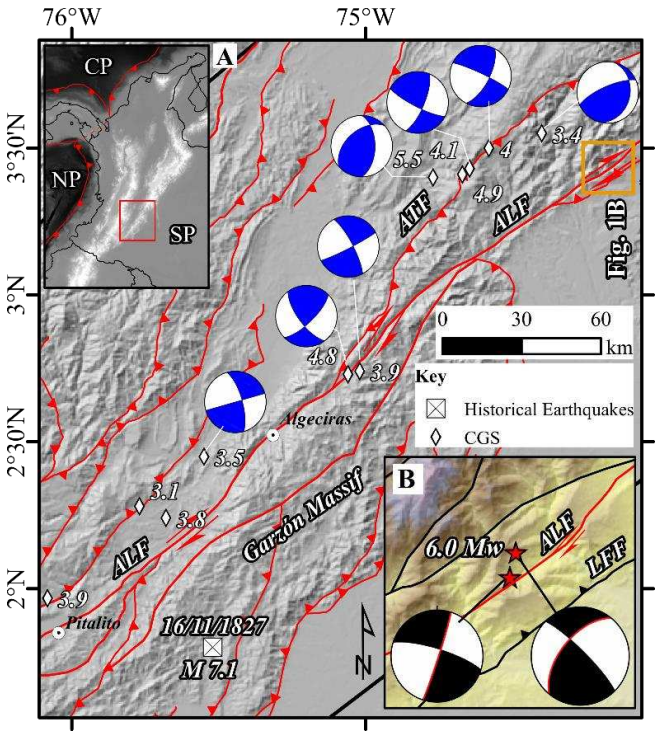

Figure 1. A. Shaded relief map showing the regional location of the study area and the northern segment of the Algeciras Fault (ALF). Focal mechanisms of shallow earthquakes (< 50 km) represented as conventional "beachball" plots (white quadrants for extensional while black quadrants for compressive). Inset in the upper-left corner shows the location of panel A in the Colombian Andes. ATF = Altamira Fault; NP = Nazca Plate; CP = Caribbean Plate; SP = South American Plate. B. Location of the Mesetas Earthquake in the Mesetas area, its main aftershock and the beachball plots for each event. LFF = La Florida Fault. The fault pattern was obtained from Gómez et al. (2019).

2 STUDY AREA

2.1 Tectonic and geological background

The study area is located on the eastern foothills of the Colombian Eastern Cordillera (Figure 1). This range, considered as a by-verging tectonic inverted Mesozoic Basin (Cooper et al., 1995; Mora et al., 2006), is characterized by composite thick and thin skin tectonic styles. The southern segment of the orogen is a narrow range bounded in the southeast by the Algeciras Fault (ALF), a right-lateral strike-slip fault with a minor reverse component observed along local restraining bends (Taboada et al., 2000; Velandia et al., 2005). According to Velandia et al. (2005), the oblique convergence of the two main slabs in the Colombian region (Nazca and South American Plates) is accommodated trough the ALF (Figure 1).

The ALF has a remarkable topographic expression that extends for more than 800 km from the central Eastern Cordillera in Colombia into Ecuador (Acosta et al., 2007; Velandia et al., 2005).

Along with the ALF, the Altamira Fault (ATF) accommodates dip-slip strain, creating thus a faulted block that widens for about 30 km (Figure 1). It is in this faulted block where the Mesetas Earthquake struck (Figure 1B), probably associated with a rupture of the ALF. According to the focal mechanisms of the event and the main aftershock (Figure 1B), the seismogenic fault has a right-lateral strike-slip kinematics and southeast vergence, matching with the expected geometry and kinematics of the ALF. Likewise, focal mechanisms compiled from the Colombian Geological Survey (CGS, Figure 1), show a strike-slip pattern with some reverse-type ruptures, suggesting a transpressive stress state for most of the study area (Figure 1A). This area has been widely recognized with high seismic hazard given the historical events reported, such as the Villavicencio Earthquake on August 31, 1917 (Mw = 6.7) (Cifuentes and Sarabia, 2006).

Geologically, the study area is mainly composed of Cambrian to Devonian sedimentary rocks with slight signals of metamorphism, especially those rocks at the base of the sequence. As it is observed in Figure 2, most of the landslides were concentrated on the Cambrian Guape-Duda Formation. This unit is composed of sandstones interbedded with black mudstones, whereas polymictic conglomerates are subordinated (SGC, 2015). Along with the Guape-Duda Formation, the Lutitas de Pipiral and San Fernando formations were also affected by EQTLs (Figure 2).

The Lutitas de Pipiral Formation is mainly composed of reddish and greenish mudstones interbedded with quarzitic sandstones of Devonian age (SGC, 2015). Finally, the San Fernando Formation corresponds to a Paleogene fine-grained sequence composed of grey claystone interbedded with quartz sandstones and localized coal beds (SGC, 2015).

3 LANDSLIDE INVENTORY

3.1 Methods

The EQTL inventory for the Mesetas event was constructed with the criteria developed by Harp et al. (2011), and Tanyaş et al. (2017) for evaluating the reliability of an inventory:

i. The inventory should cover the entire affected area.

ii. Mapping all the landslides triggered after the earthquake independent of their sizes.

iii. Map every landslide as a polygon instead of a point.

iv. As possible, define if the landslides were triggered before or after the earthquake.

v. Classify each landslide, at least in their type.

vi. Validate the landslide inventory according to field observations.

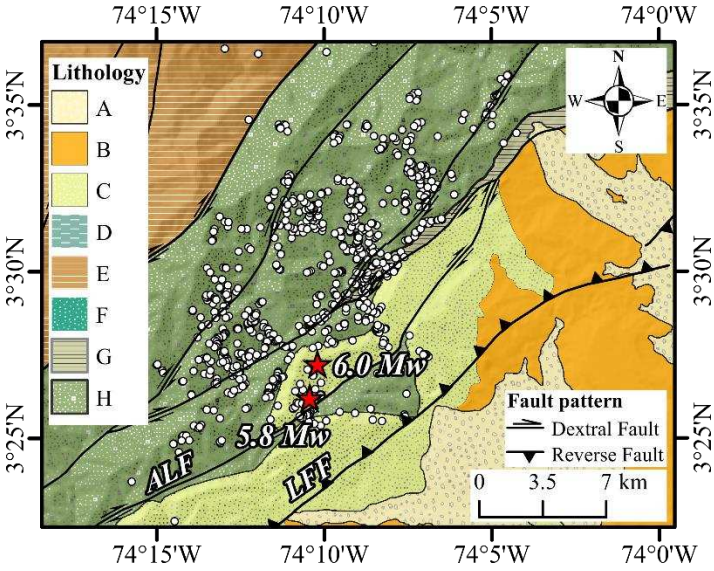

Figure 2. Generalized geological map of the study area. Modified from SGC (2015). The Mesetas Earthquake epicenter and the main aftershock are represented as red markers. The white markers correspond to the EQTLs. A = Quaternary; B = San Fernando Fm.; C = Palmichal Fm; D = Capas Rojas de Guatiquía Fm.; E = Lutitas de Pipiral Fm.; F = Güejar Group; G = Ariari Fm.; H = Guape-Duda Fm. Faults abbreviations as in Figure 1.

Accordingly, a supervised inventory for the Mesetas Earthquake was obtained by analyzing pre- and post-earthquake multi-spectral satellite imagery (Table 1) from Sentinel 2, PlanetScope (https://www.planet.com/) and a medium-resolution Digital Elevation Model (DEMs). For mapping the Mesetas inventory, true-color, and infrared-color composite images were used, focusing on identifying individual slope failures even if they were amalgamated. Avoiding amalgamated features is critical when a statistical analysis for an inventory is preferred, preventing then some artifacts in data analysis such as volume overestimation (Marc and Hovius, 2015).

3.2 Size-frequency distribution

The size-frequency distribution of the Mesetas inventory was analyzed by studying the total area and total volume of EQTLs from the Mesetas

Earthquake. In total, 838 individual landslides were mapped using the criteria exposed above. In terms of areas, a mean landslide area of 2.75×10^{-3} km^2 was calculated, which is reasonably similar to the expected average area for an EQTL (3.07×10^{-3} km^2), according to Malamud et al. (2004).

Table 1. List of satellite imagery used to obtain the Mesetas inventory

Sensor	Acquisition date	Resolution (m)
Pre-earthquake		
PlanetScope	4/10/2019	3.6
	7/10/2019	3.8
	4/11/2019	3.5
Sentinel 2	25/12/2018	10
	13/02/2019	
	3/07/2019	
Post-earthquake		
PlanetScope	8/01/2020	3.6
	10/01/2020	3.6
Sentinel 2	4/01/2020	10
	9/01/2020	

Based on these individual landslides area, the total affected area by landslides following the Mesetas Earthquake is about 2.31 km^2. If this value is compared with the expected affected area by landslides proposed by Keefer (2002) using the event magnitude ($\log_{10}A = M - 3.46(\pm 0.47)$), the Mesetas Earthquake is within two and three orders of magnitudes less. Then, caution should be taken, at least in strike-slip earthquakes, when estimating the total affected area by landslides using the event magnitude as the primary proxy. Clearly, this procedure would lead to overestimations of the total affected area.

In terms of remobilized material, an empirical formula to obtain the landslide volume (Larsen et al., 2010) was used: $V = 0.146A^{1.35}$, where A is the landslide area for each entity. Based on this equation, this work obtained a mean landslide volume of 8096 m^3 and a total event volume of 6.79×10^{-3} km^3. This value is slightly higher than the upper bound expected for an earthquake with magnitude 6, according to the correlations proposed by Malamud et al. (2004).

The landslide concentration (LC) defined as the number of landslides per square kilometer was computed for the Mesetas Earthquake. Given that 838 landslides were inventoried over an area of ~1500 km^2, the average landslide concentration equals to 0.56/km^2. This value is slightly higher if compared to other earthquakes with magnitudes over 6.5 as the Loma Prieta (LC = 0.42 – 0.54; Keefer, 2000), or the Inangahua (LC = 0.40; Parker et al., 2015) earthquakes. As is shown in Figure 3, the highest concentrations are restricted to the hanging wall of the ALF, particularly between the Río Tonoa and the Guapecito Faults. Besides, most peaks are located N-NE of the epicenter, which may suggest that the rupturing direction (right-lateral faulting towards the NE) may play some control on landslide location.

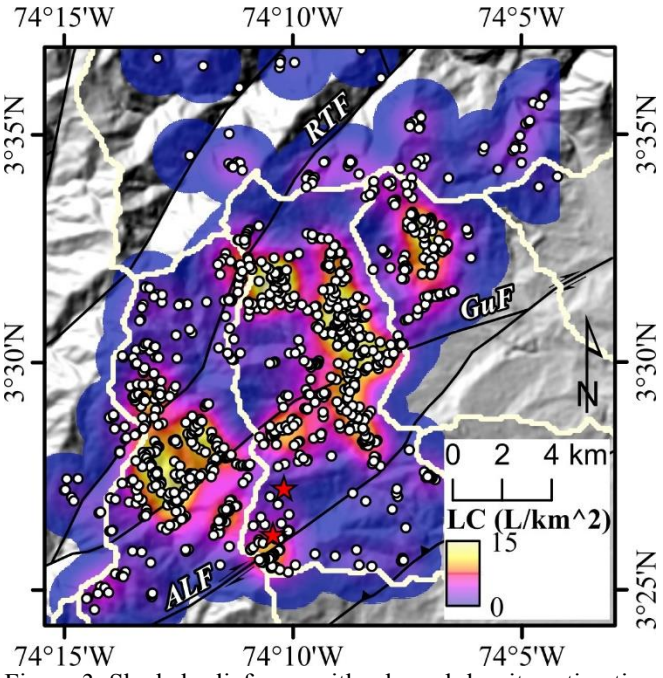

Figure 3. Shaded relief map with a kernel density estimation of landslide concentration for the Mesetas Inventory. GuF = Guapecito Fault; RTF = Río Tonoa Fault

The relationship between LC and the epicentral distance was determined using a series of concentric bands of 1 km wide extending from the source (e.g., Gorum et al., 2011). For each band, the area and the number of landslides were computed (Figure 4). As shown in Figure 4, LC decreases as the distance to epicenter increases, however, several peaks were observed (e.g., between the epicentral distance of 1-2, 2-3, 4-5, 6-7, 12-13 and 15-16).

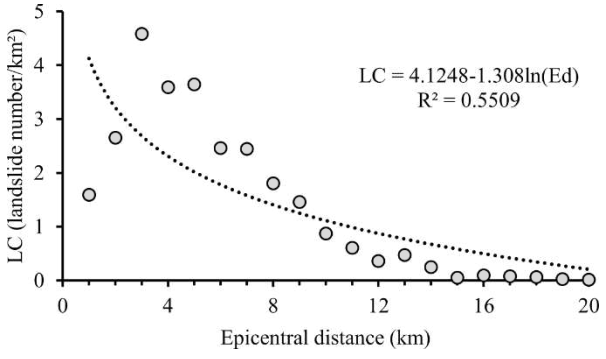

Figure 4. Relationship between landslide concentration and distance from epicenter for the Mesetas Earthquake.

Then, opposed to other studies (e.g., Keefer, 2000; Mahdavifar et al., 2006; Sepúlveda et al., 2010), we did not found a strong correlation between LC and distance from the epicenter. Hence, other controlling parameters dominate the distribution and location of EQTLs for this event rather than the epicentral distance.

3.3 Controlling parameters: terrain and seismic variables

Six terrain factors, including the elevation, slope, local relief, slope position, slope aspect, and curvature, were computed for the Mesetas inventory. All the metrics were extracted from a 1 arc-second Shuttle Radar Topography Mission (SRTM) DEM provided by NASA and calculated using different tools available at ESRI ArcGIS version 10.6.

The local relief factor was obtained after subtracting the minimum elevation from the maximum elevation on a circular-moving window with a radius of 1 km. In order to explore any topographic influence on landslide triggering, we calculated the slope position using the Topographic Position Index (TPI) (Weiss, 2001) with the aim of the Land facet corridor extension for ESRI ArcGIS (Jenness, 2013). This index compares the mean elevation in the vicinity of a cell using neighborhood statistics. Along with the TPI, the tool also takes into account the surface slope to assign a composite classification as follows: valleys, lower slope, gentle slope (TPI value around 0, slope angle ≤ 5°), steep slope (TPI value around 0, slope angle > 5°), upper slope, and ridge (extreme high TPI value) (Weiss, 2001).

The slope aspect refers to the downslope direction of the surface in azimuthal degrees. In this work, the slope orientation was categorized as follows: N (337.5 – 22.5), NE (22.5 – 67.5), E (67.5 – 112.5), SE (112.5 – 157.5), S (157.5 – 202.5), SW (202.5 – 247.5), W (247.5 – 292.5), and NW (292.5 – 337.5). In such cases where there is a flat surface, the assigned value is -1. The curvature refers to the plan curvature, which relates to the convergence and divergence of flow across the hillslope. Positive curvature values suggest the slope surface is convex, whereas a negative curvature suggests the opposite, i.e., the surface is concave. Curvature values close to zero suggest the slope is planar and straight. We complemented this analysis focused on understanding the relationship between landslides with the distance to the seismogenic fault (Algeciras Fault).

3.3.1 Results and interpretation

The results of the terrain variables analysis are shown in Figures 5 and 6.

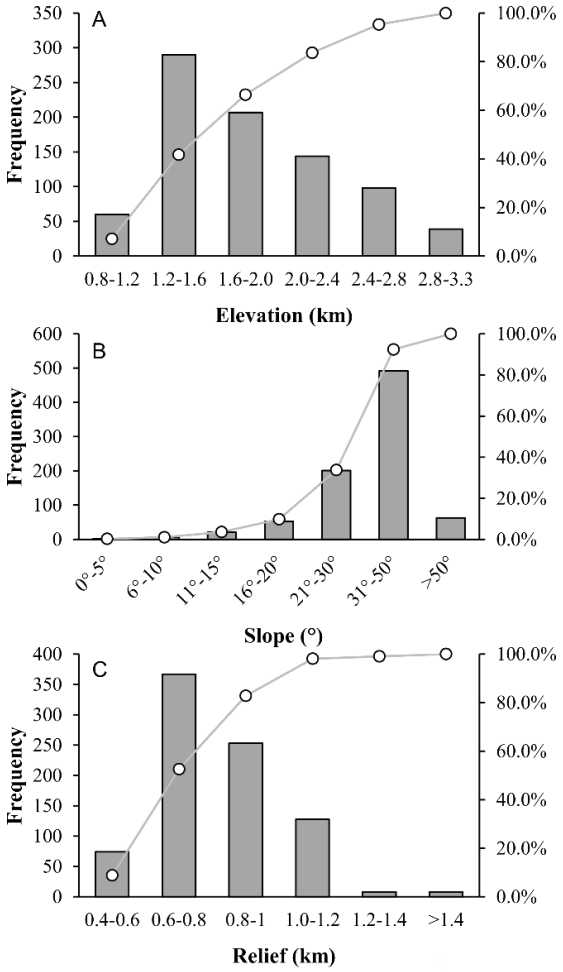

Figure 5. Frequency histograms for three of the terrain variables analyzed in this work. (A) Elevation, (B) slope, (C) local relief. The line corresponds to the accumulated frequency.

In terms of elevation, most of the landslides were triggered between 1200-1600 m, whereas the highest elevations (> 2800 m) showed the least frequency, reaching only 5% of the landslides. The mean elevation for the dataset is about 1825 m, slightly higher than the most abundant class. Otherwise, the initiation points were preferably located on steep slopes ranging from 31°-50° (~59%) and hillslopes with local relief values ranging between 600-800 m (44%), with a second significant cluster between 800-1000 m (30%). The mean slope calculated was about 35°, which is higher than the expected angle stability for materials (e.g., Burbank et al., 1996).

The TPI shows two main patterns regarding the preferred location of the initiation points (Figure

6A). Most of the landslides were triggered either closer to the valleys (49%) or nearby the ridges (47%). In terms of the preferred slope orientation, the E-SE-S quadrant concentrated about 69% of the landslides, mainly those slopes trending towards the SE (Figure 6B), which is almost orthogonal to the seismogenic fault (Figure 1). Finally, the plan curvature gave slightly suggesting results pointing to concave slopes as the more prone to landsliding (negative values accumulated about 51% of the landslides, Figure 6C).

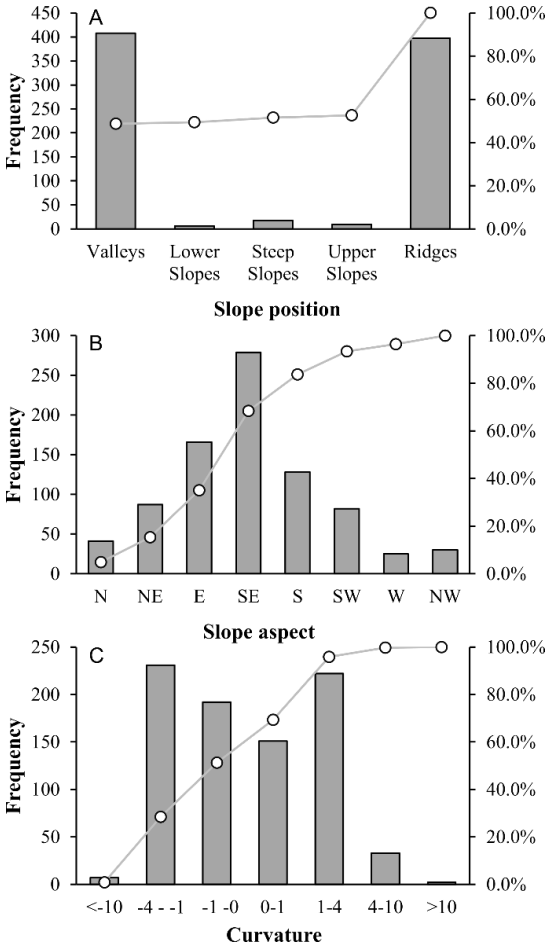

Figure 6. Frequency histograms for the (A) slope position index; (B) slope aspect, and (C) the plan curvature. The line corresponds to the accumulated frequency.

The results of the seismic parameters evaluated in this work are shown in Figures 4 and 7. The distance to the seismogenic fault analysis gave similar peaks as the distance to epicenter analysis (Figure 4), particularly in class 4-6 km with about 240 processes (Figure 7). As it is observed in Figure 3, these peaks are closely related to the fault trace of the Guapecito Fault, a subsidiary structure of the ALF.

4 DISCUSSION

Based on the results presented above, it is reasoned that the EQTLs following the Mesetas Earthquake are primarily controlled by terrain variables such as slope and local relief. The observed distribution suggests that most of the processes are restricted to the fault rupture area near the seismogenic fault, and their spatial extent is restricted to the upthrown block of the ALF. As observed in Figure 3, this distinct "hanging wall effect" accounts for most of the EQTLs and the highest concentration areas. Such a similar pattern has also been observed in other seismic events like the Kashmir (Sato et al., 2007), Iwate-Miyagi (Yagi et al., 2009), or the Lushan (Xu and Xu, 2014) earthquakes. This finding is valuable to better constraint the expected landslide distribution on similar earthquakes related to oblique faults as the ALF.

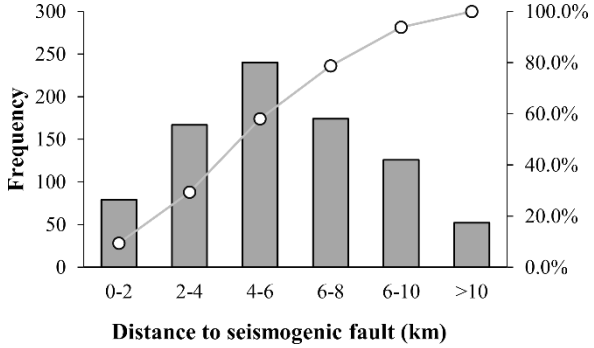

Figure 7. Frequency histogram for the distance to seismogenic fault seismic parameter. The line corresponds to the accumulated frequency.

In regards to the landslide position, a bimodal distribution was observed. Most of the landslides were frequent on valleys and lower slopes. This pattern was also recognized in the Port-Au-Prince Earthquake (Xu et al., 2014) and, more recently, after the Hokkaido Earthquake (Wang et al., 2019). According to these authors, river downcutting and bank failure on unstable, highly weathered, and sheared materials is a primary conditioning factor for landsliding in this area. On the other hand, a significant group of landslides was triggered near or at the ridges. Besides, this cluster of landslides also correlates with steep slopes (>35°); their location strongly suggests that some topographic site effects acted and controlled landslide distribution (Meunier et al., 2008).

In strike-slip earthquakes, as the Mesetas Earthquake, it has been observed that landslides cluster around slopes oriented parallel to the co-seismic slip direction (e.g., Gorum et al., 2014; Xu et al., 2014; Barlow et al., 2015). However, according to the observations made, landslides cluster on SE-facing slopes, perpendicular to the expected co-seismic slip for a right-lateral fault. This may indicate that another key factor is

controlling landslide occurrence following the Mesetas Earthquake. Rapid inspection of the inventoried landslides revealed that most landslides facing SE are located on structurally-controlled slopes by the Guapecito Fault (Figure 3). This structure is also closely related to the calculated peaks in landslide concentration versus distance to the epicenter and the seismogenic fault (Figures 3 and 7). This cumulative evidence is highly indicative of a robust tectonic control on EQTL location in this part of the orogen. Several authors (e.g., Owen et al., 2008) have observed that the rock mass strength exerts a primary control on EQTLs.

Furthermore, in seismogenic active areas with recurring earthquakes, seismic ground motion profoundly weakens the parental material, enhancing hillslope instability (Parker et al., 2015). This tectonic weakening, characteristic of strike-slip shear zones such as the Alpine Fault Zone (Korup, 2004), strongly influences the dynamic response of hillslopes after recurring earthquakes. For the Mesetas area, it could be then reasonable to interpret that the faulted block between the ALF and Río Tonoa Fault corresponds to a right-lateral shear zone where repeated historical earthquakes have weakened the parental material, controlling not only landslide distribution but their location on structurally-controlled slopes (SE-facing ones).

5 SUMMARY AND CONCLUSIONS

This work presents here the first comprehensive analysis of an EQTL inventory for the Colombian Andes in northwest South America. In total, 838 individual landslides extending for an area of 2.31 km^2 were mapped. Based on the analysis of well-known relationships between earthquake magnitude and expected total affected area (e.g., Keefer 2002), we find no obvious correlation and caution should be taken when using this fit to constraint the magnitude of the event. For the Mesetas inventory, these relationships gave an overestimation of at least two orders of magnitude in the expected affected area, and thus, other controlling parameters different to the event magnitude should be evaluated.

Looking at the terrain factors, we observed that most EQTLs occurred on middle elevations with high topographic slopes (mean slope of 35°) and concave slopes where groundwater may accumulate and promote slope failure. In terms of the TPI, EQTLs were distributed fairly homogeneous on valleys and ridges, suggesting that river incision and topographic amplification may have worked to control landslide location.

Finally, but not least, structure and lithology, along with the steepest topography, are considered as the main factors contributing to the occurrence of EQTLs in the study area. Accordingly, peaks in landslide concentration and the orientation of the main failures were controlled by the shear zone bounded by the Guapecito Fault, a subsidiary branch of the ALF. It is thus inferred that tectonic weakening on the parental material, probably accumulated after the seismic shaking of past earthquakes, is the main factor controlling the occurrence of EQTLs.

6 REFERENCES

Acosta, J., Velandia, F., Osorio, J., Lonergan, L., Mora, H., (2007). *Strike-slip deformation within the Colombian Andes*. Geol. Soc. London, Spec. Publ. 272: 303–319.

Barlow, J., Barisin, I., Rosser, N., Petley, D., Densmore, A., Wright, T., (2015). *Seismically-induced mass movements and volumetric fluxes resulting from the 2010 Mw=7.2 earthquake in the Sierra Cucapah, Mexico*. Geomorphology 230: 138–145.

Bird, J.F., Bommer, J.J., (2004). *Earthquake losses due to ground failure*. Eng. Geol. 75: 147–179.

Budimir, M.E.A., Atkinson, P.M., Lewis, H.G., (2014). *Earthquake-and-landslide events are associated with more fatalities than earthquakes alone*. Nat. Hazards 72: 895–914.

Burbank, D.W., Leland, J., Fielding, E., Anderson, R.S., Brozovic, N., Reid, M.R., Duncan, C., (1996). *Bedrock incision, rock uplift and threshold hillslopes in the northwestern Himalayas*. Nature 379: 505-510.

Cifuentes, H., Sarabia, A.M., (2006). *Estudio macrisísmico del sismo del 31 de Agosto de 1917, Villavicencio (Meta)*. INGEOMINAS: pp. 146.

Cooper, M. A., Addison, F.T., et al., (1995). *Basin development and tectonic history of the Llanos Basin, Eastern Cordillera, and Middle Magdalena Valley, Colombia*. American Association of Petroleum Geologists Bulletin 79: 1421–1443.

Forero-Dueñas, C., (1996). *Experiences from the Páez Earthquake, Colombia*, in: Eleventh World Conference on Earthquake Engineering. p. 8.

Froude, M.J., Petley, D.N., (2018). *Global fatal landslides 2004 to 2016*. Nat. Hazards Earth Syst. Sci. 18: 2161–2181.

Gómez, J., Schobbenhaus, C., Montes, N., (compilators) (2019). Geological Map of South America. Scale 1:5000000.

Gorum, T., Fan, X., van Westen, C.J., Huang, R.Q., Xu, Q., Tang, C., Wang, G., (2011). *Distribution pattern of earthquake-induced landslides triggered by the May 12 2008 Wenchuan earthquake*. Geomorphology 133: 152–167.

Gorum, T., Korup, O., van Westen, C.J., van der Meijde, M., Xu, C., van der Meer, F.D., (2014). *Why so few? Landslides triggered by the 2002 Denali earthquake, Alaska*. Quat. Sci. Rev. 95: 80–94.

Harp, E.L., Keefer, D.K., Sato, H.P., Yagi, H., (2011). *Landslide inventories: The essential part of seismic landslide hazard analyses*. Eng. Geol. 122: 9–21.

Instituto de Investigaciones en Geociencias, Minería y Química (INGEOMINAS), (1996). *Estudio de Amenazas y Zonificación Geológica de la Cuenca del Río Páez – Fase I: Informe Final*. Bogotá D.C., Colombia, pp. 169.

Jenness, J., 2013. *Topographic Position Index (TPI): an ArcView 3.X tool for analyzing the shape of the landscape*.

Keefer, D.K., (2000). *Statistical analysis of an earthquake-induced landslide distribution - The 1989 Loma Prieta, California event*. Eng. Geol. 58: 231–249.

Keefer, D.K., (2002). *Investigating landslides caused by earthquakes - A historical review*. Surv. Geophys. 23: 473–510.

Korup, O., (2004). *Geomorphic implications of fault zone weakening: Slope instability along the alpine fault, South Westland to Fiordland*. New Zeal. J. Geol. Geophys. 47: 257–267.

Larsen, I.J., Montgomery, D.R., Korup, O., (2010). *Landslide erosion controlled by hillslope material*. Nat. Geosci. 3: 247–251.

Mahdavifar, M.R., Solaymani, S., Jafari, M.K., (2006). *Landslides triggered by the Avaj, Iran earthquake of June 22, 2002*. Eng. Geol. 86: 166–182.

Malamud, B.D., Turcotte, D.L., Guzzetti, F., Reichenbach, P., (2004). *Landslides, earthquakes, and erosion*. Earth Planet. Sci. Lett. 229: 45–59.

Marano, K.D., Wald, D.J., Allen, T.I., (2010). *Global earthquake casualties due to secondary effects: A quantitative analysis for improving rapid loss analyses*. Nat. Hazards 52: 319–328.

Marc, O., Hovius, N., (2015). *Amalgamation in landslide maps: effects and automatic detection*. Nat. Hazards Earth Syst. Sci. 15: 723-733.

Mayorga, E., Dionicio, V., Lizarazo, M., Pedraza, P., et al., (2020). *El sismo de Mesetas, Meta del 24 de diciembre de 2019. Aspectos sismológicos y movimiento fuerte.* Internal report: 1-56.

Meunier, P., Hovius, N., Haines, J.A., (2008). *Topographic site effects and the location of earthquake induced landslides*. Earth Planet. Sci. Lett. 275: 221–232.

Mora, A., Parra, M., Strecker, M.R., Kammer, A., Dimaté, C., Rodríguez, F., (2006). *Cenozoic contractional reactivation of Mesozoic extensional structures in the Eastern Cordillera of Colombia*. Tectonics 25: 1–19.

Owen, L.A., Kamp, U., Khattak, G.A., Harp, E.L., Keefer, D.K., Bauer, M.A., (2008). *Landslides triggered by the October 8 2005 Kashmir earthquake*. Geomorphology 94: 1–9.

Parker, R.N., Hancox, G.T., Petley, D.N., Massey, C.I., Densmore, A.L., Rosser, N.J., (2015). *Spatial distributions of earthquake-induced landslides and hillslope preconditioning in the northwest South Island, New Zealand*. Earth Surf. Dyn. 3: 501–525.

Rodríguez, C.E., Bommer, J.J., Chandler, R.J., (1999). *Earthquake-induced landslides: 1980-1997*. Soil Dyn. Earthq. Eng. 18: 325–346.

Servicio Geológico Colombiano (SGC) (2015). *Geología de la Plancha 304 La Uribe*. Scale 1:100,000.

Sato, H.P., Hasegawa, H., Fujiwara, S., Tobita, M., Koarai, M., Une, H., Iwahashi, J., (2007). *Interpretation of landslide distribution triggered by the 2005 Northern Pakistan earthquake using SPOT 5 imagery.* Landslides 4: 113–122.

Sepúlveda, S.A., Serey, A., Lara, M., Pavez, A., Rebolledo, S., (2010). *Landslides induced by the April 2007 Aysén Fjord earthquake, Chilean Patagonia*. Landslides 7: 483–492.

Taboada, A., Rivera, L.A., Fuenzalida, A., Cisternas, A., Philip, H., Bijwaard, H., Olaya, J., Rivera, C., (2000). *Geodynamics of the northern Andes: Subductions and intracontinental deformation (Colombia)*. Tectonics 19: 787–813.

Tanyaş, H., van Westen, C.J., Allstadt, K.E., Anna Nowicki Jessee, M., Görüm, T., Jibson, R.W., Godt, J.W., Sato, H.P., Schmitt, R.G., Marc, O., Hovius, N., (2017). *Presentation and Analysis of a Worldwide Database of Earthquake-Induced Landslide Inventories*. J. Geophys. Res. Earth Surf. 122: 1991–2015.

Velandia, F., Acosta, J., Terraza, R., Villegas, H., (2005). *The current tectonic motion of the Northern Andes along the Algeciras Fault System in SW Colombia*. Tectonophysics 399: 313–329.

Wang, F., Fan, X., Yunus, A.P., Siva Subramanian, S., Alonso-Rodriguez, A., Dai, L., Xu, Q., Huang, R., (2019). *Co-seismic landslides triggered by the 2018 Hokkaido, Japan (Mw 6.6), earthquake: spatial distribution, controlling factors, and possible failure mechanism*. Landslides 16: 1551–1566.

Weiss, A., (2001). *Topographic position and landforms analysis*, in: ESRI User Conference. San Diego, California.

Xu, C., Shyu, J.B.H., Xu, X., (2014). *Landslides triggered by the January 12 2010 Port-au-Prince, Haiti, Mw = 7.0 earthquake: Visual interpretation, inventory compiling, and spatial distribution statistical analysis*. Nat. Hazards Earth Syst. Sci. 14: 1789–1818.

Xu, C., Xu, X., (2014). *The spatial distribution pattern of landslides triggered by the April 20 2013 Lushan earthquake of China and its implication to identification of the seismogenic fault*. Chinese Sci. Bull. 59: 1416–142.

Yagi, H., Sato, G., Higaki, D., Yamamoto, M., Yamasaki, T., (2009). *Distribution and characteristics of landslides induced by the Iwate-Miyagi Nairiku Earthquake in 2008 in Tohoku District, Northeast Japan*. Landslides 6: 335–344.